Sensing and Bio-Sensing Research 25 (2019) 100297

Contents lists available at ScienceDirect

Sensing and Bio-Sensing Research

journal homepage: www.elsevier.com/locate/sbsr

Mathematical modeling of interactions of cabergoline with human serum albumin for biosensing of human serum albumin

Ali R. Jalalvand[a,*], Sirous Ghobadi[b], Vali Akbari[b,c], Hector C. Goicoechea[d], Elahe Faramarzi[a], Majid Mahmoudi[a]

[a] Research Center of Oils and Fats, Kermanshah University of Medical Sciences, Kermanshah, Iran
[b] Department of Biology, Faculty of Science, Razi University, Kermanshah, Iran
[c] Medical Biology Research Center, Health Technology Institute, Kermanshah University of Medical Sciences, Kermanshah, Iran
[d] Laboratorio de Desarrollo Analítico y Quimiometría (LADAQ), Catedra de Química Analítica I, Universidad Nacional del Litoral, Ciudad Universitaria, CC242 (S3000ZAA), Santa Fe, Argentina

ARTICLE INFO

Keywords:
Cabergoline
Human serum albumin
Multivariate analysis
Interactions
Determination

ABSTRACT

In this work, we are going to study the interactions of cabergoline (CBG) with human serum albumin (HSA) by mathematical modeling of voltammetric and spectroscopic data. To achieve this goal, voltammetric and spectroscopic data will be augmented into a data matrix which will be resolved by multivariate curve resolution-alternating least squares (MCR-ALS) as a powerful chemometric tool. Then, the quality of the data fitting by MCR-ALS will be examined by MCR-BANDS to ensure about the absence of the rotational ambiguities in the results. Molecular docking will also be used to model the interactions of CBG with HSA for verifying the results obtained from experimental methods. Hard-modeling of the experimental data will be performed by EQUISPEC to compute the binding constant of the complex formed from the interactions of CBG with HSA for verifying the binding constant obtained by direct analysis of the experimental data. Finally, two chrono-amperometric measurements based on CBG-HSA interactions will be performed to develop a novel electroanalytical method for determination of electro-inactive HSA.

1. Introduction

Cabergoline (CBG, Fig. 1A) an ergot derivative, is a long-acting dopamine agonist and prolactin inhibitor. It is used to treat hyperprolactinemic disorders and Parkinsonian Syndrome [1]. It acts by direct stimulation of the D2-dopamine receptors on pituitary lactotrophs, thus inhibiting Prolactin secretion.

Human serum albumin (HSA, Fig. 1B) as the most abundant protein in blood plasma can act as a shuttle for small molecules [2–8]. Therefore, free concentration and distribution of the small molecules are depended on their interactions with HSA. According to the information mentioned above, it is important to investigate the interactions of drugs with HSA. It should be noted that unusual concentrations of HSA in blood serum is an important factor for detection of some diseases, therefore, determination of HSA in blood serum is important. Common techniques for determination of HSA are included capillary electrophoresis, immunoassays, LC-MS/MS and surface enhanced Raman scattering which are expensive and time-consuming. Therefore, developing new analytical techniques for determination of HSA which are simple and mow-cost are highly demanded.

Common methods for investigation of drug-HSA interactions are including UV–Vis spectrophotometry [9], FT-IR [10], electrochemistry [11], capillary electrophoresis [12], HPLC [13], and NMR [14] and some of them have been assisted by chemometric methods by the other researchers [15,16]. HSA-drug interaction is a complex system and its monitoring is complicated because free drug, free HSA and their complex product must be simultaneously monitored. Therefore, investigation of HSA-drug interaction must be assisted by chemometric methods. Multivariate curve resolution-alternating least squares (MCR-ALS) is a powerful chemometric tool which is able to the simultaneous analysis of the data with different origins to obtain valuable information about the studied system which cannot be obtained by the use of conventional methods. Therefore, we will use MCR-ALS for further analysis of CBG-HSA interactions.

The steps of our study will be: 1) investigation of interactions of CBG with HSA by direct analysis of voltammetric and spectroscopic data, 2) using voltammetric and spectroscopic data to build an augmented data matrix as the input of MCR-ALS to obtain new information

* Corresponding author.
E-mail address: alireza.jalalvand@kums.ac.ir (A.R. Jalalvand).

https://doi.org/10.1016/j.sbsr.2019.100297
Received 14 June 2019; Received in revised form 30 July 2019; Accepted 6 August 2019

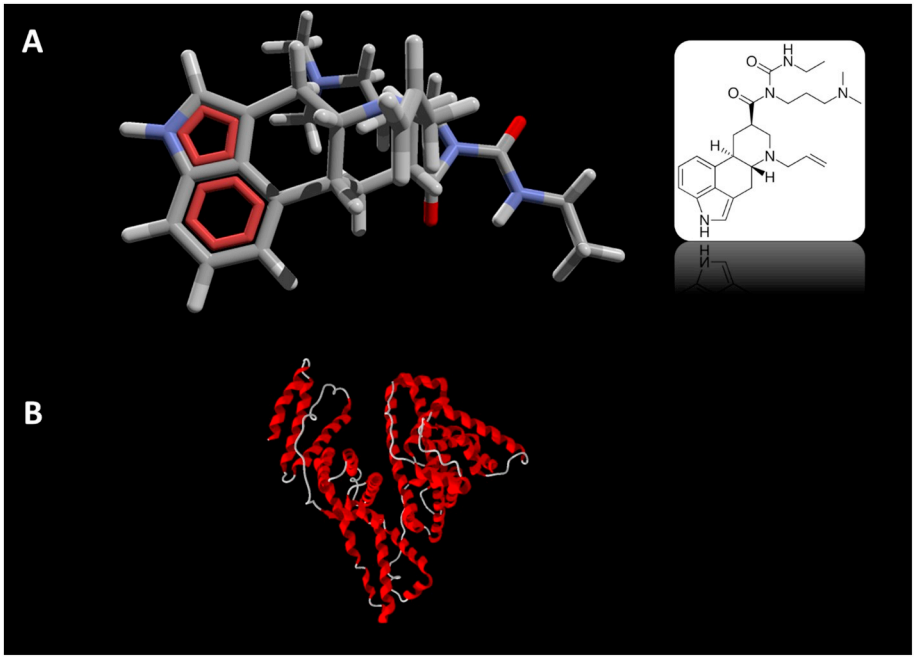

Fig. 1. (A) Molecular structure of CBG and (B) secondary structure of HSA.

about CBG-HSA interactions, 3) modeling of CBG-HSA interactions by molecular modeling methods and 4) developing a novel electroanalytical methodology based on CBG-HSA interactions for determination of HSA.

2. Experimental and theoretical details

2.1. Experimental details

2.1.1. Chemicals and solutions

HSA, CBG, warfarin (Wr), ibuprofen (Ip), acetic acid, ethanol, dimethylformamide (DMF), sodium phosphate monobasic (NaH_2PO_4), sodium phosphate dibasic (Na_2HPO_4), 1-ethyl-3-methylimidazolium bis (trifluoromethylsulfonyl)Imide (IL), dimethyl sulfoxide (DMSO), sodium hydroxide, phosphoric acid (H_3PO_4), and hydrochloric acid were purchased from Sigma. Ionic Liquid Technologies supported us for preparing multiwalled carbon nanotubes (MWCNTs). Other chemicals were prepared from legal sources. A phosphate buffer solution (PBS) with a concentration of 0.05 M, pH at 7.4 was prepared and used as the medium of the interactions. Stock solutions of CBG (0.1 M) and HSA (0.01 M) were prepared in PBS (0.05 M, pH at 7.4) and kept in a refrigerator. Stock solutions of Wr (0.1 M) and Ip (0.1 M) were prepared in DMSO. 20 mg MWCNTs was dissolved in 1 mL DMF containing 30 µL IL and ultrasonicated for 30 min to obtain a homogeneous gel-like MWCNTs-IL solution.

Three human serum samples were prepared from a medical diagnostic laboratory and centrifuged at 4500 rpm for 20 min and then, 5 mL of each sample was diluted with 45 mL PBS (0.05 M, pH 7.4). For HSA determination, each sample was amperometrically analysed.

2.1.2. Instruments and softwares

All the electrochemical data were recorded by an Autolab PGSTAT302N-high performance controlled by the NOVA 2.1.2 software. Electrochemical measurements were performed by a bare or modified glassy carbon electrode (GCE), a Pt wire and an Ag/AgCl electrode acted as working, counter and reference electrode, respectively. A KYKY-EM 3200 scanning electron microscope was used to capture the SEM image. A Cary Eclipse fluorescence spectrophotometer equipped with a water bath and a 1.0 cm quartz cell was used to record the spectrofluorimetric data and a Shimadzu spectrophotometer equipped with a 1.0 cm quartz cell was used to record the spectrophotometric data. An ELMEIRON pH-meter (CP-411) was used to adjust the pH of the solutions. The molecular structure of the CBG was constructed by Hyperchem package (Version 8.0) and the PDB file of HSA (PDB Id: 1AO6) was downloaded from the internet. The Molegro virtual docker (MVD) software was used to dock CBG with HSA. LIGPLOT [17], was used to plot the interactions of CBG and HSA. The m-files of MCR-ALS and MCR-BANDS were downloaded from the internet [18].

2.1.3. Fabrication of the modified electrodes

To fabricate the HSA/GCE, 12 µL HSA (10^{-5} M) was drop-casted onto the surface of the cleaned GCE and dried at room temperature. To fabricate MWCNTs-IL/GCE, 10 µL MWCNTs-IL was drop-casted onto the surface of the cleaned GCE and dried at room temperature. The SEM images captured from the surface of HSA/GCE and MWCNTs-IL/GCE are shown in Fig. 2.

2.1.4. Procedures

Spectroscopic experiments were performed in a quartz cell. For each experiment, HSA or CBG was added step-by-step to a quartz cell containing 2 mL of HSA or CBG while the added volume was less than 0.2 mL. Spectroscopic titrations were performed by manual shanking where each solution was allowed to be equilibrated for 15 s.

In voltammetric experiments, 5 mL of HSA or CBG with a known concentration was added to a cell and titrated by different volumes of HSA or CBG while the total added HSA or CBG was less than 0.5 mL. Each solution was shaken manually left to be equilibrated for 1.0 min and then, its voltammogram was recorded.

2.1.5. Experiments required to construct an augmented data matrix for the analysis by MCR-ALS

All the voltammetric and spectroscopic experiments have been coded in Table S1.

2.2. Theoretical details

2.2.1. Requirements for applying MCR-ALS to the augmented data matrix

Some works have been reported on application of MCR-ALS to the

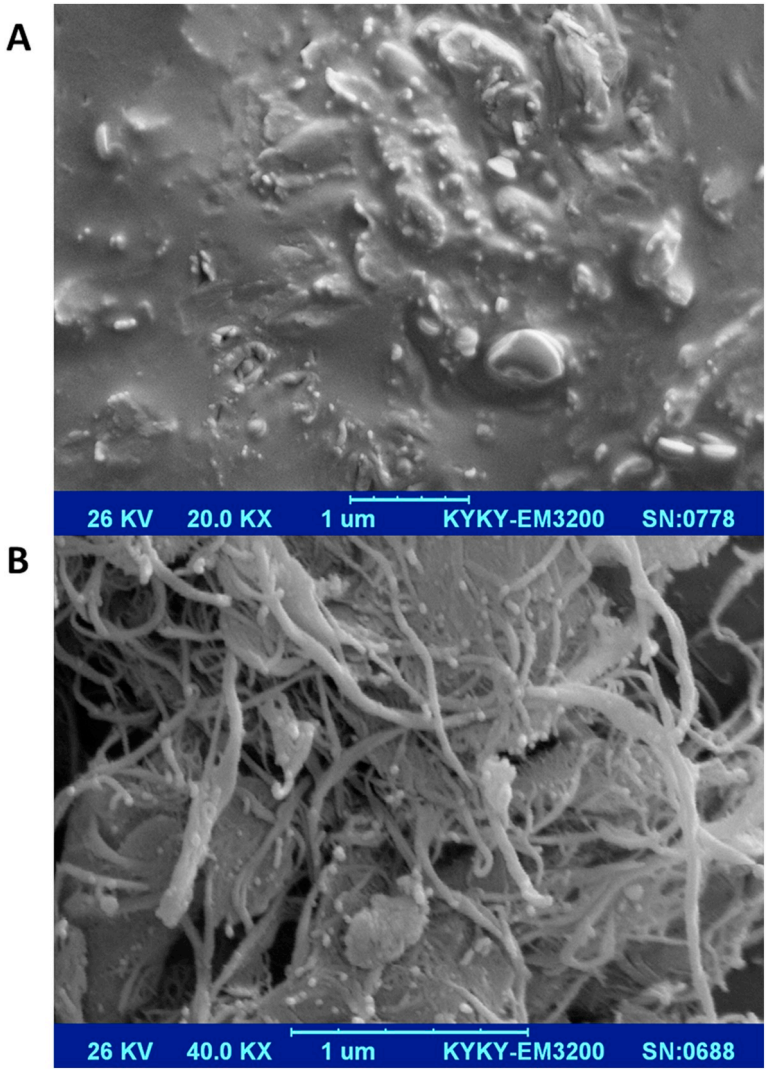

Fig. 2. The SEM image of the surface of (A) HSA/GCE and (B) MWCNTs-IL/GCE.

electroanalytical data [19–22] and in this section, a summarized description will be given. MCR can decompose a voltammetric or spectroscopic data matrix ($\boldsymbol{D}$ (M × N), M objects and N variables e.g. wavelength or potential) according to the following equation:

$$\boldsymbol{D} = \boldsymbol{C}\boldsymbol{S}^{\mathrm{T}} + \boldsymbol{E} \tag{1}$$

where $\boldsymbol{C}$ (M × P), $\boldsymbol{S}^{\mathrm{T}}$ (P × N) and $\boldsymbol{E}$ ($M \times N$) contains the concentration profiles of the P species, pure signals and residuals, respectively. ALS is an iterative approach which can be used to optimize the outputs of the MCR. MCR-ALS can also be applied to the analysis of an augmented data matrix having more than one instrumental data. In this work, CBG-HSA interactions will be studied by differential pulse voltammetry (DPV), linear sweep voltammetry (LSV), cyclic voltammetry (CV), UVVis spectrophotometry and fluorescence spectroscopy (F), and the individual instrumental data matrices were augmented as shown below:

$$\begin{bmatrix} \boldsymbol{D}_{DPV}^{CBG} \boldsymbol{D}_{\mathrm{LSV}}^{CBG} \boldsymbol{D}_{\mathrm{CV}}^{CBG} \boldsymbol{D}_{\mathrm{F}}^{CBG} \boldsymbol{D}_{\mathrm{UVVis}}^{CBG} \\ \boldsymbol{D}_{\mathrm{DPV}}^{\mathrm{HSA}} \boldsymbol{D}_{\mathrm{LSV}}^{\mathrm{HSA}} \boldsymbol{D}_{\mathrm{CV}}^{\mathrm{HSA}} \boldsymbol{D}_{\mathrm{F}}^{\mathrm{HSA}} \boldsymbol{D}_{\mathrm{UVVis}}^{\mathrm{HSA}} \end{bmatrix} = \begin{bmatrix} \boldsymbol{C}^{CBG} \\ \boldsymbol{C}^{\mathrm{HSA}} \end{bmatrix} [\boldsymbol{S}_{\mathrm{DPV}}^{\mathrm{T}} \boldsymbol{S}_{\mathrm{LSV}}^{\mathrm{T}} \boldsymbol{S}_{\mathrm{CV}}^{\mathrm{T}} \boldsymbol{S}_{\mathrm{F}}^{\mathrm{T}} \boldsymbol{S}_{\mathrm{UVVis}}^{\mathrm{T}}] + [\boldsymbol{E}_{\mathrm{DPV}} \boldsymbol{E}_{\mathrm{LSV}} \boldsymbol{E}_{\mathrm{CV}} \boldsymbol{E}_{\mathrm{F}} \boldsymbol{E}_{\mathrm{UVVis}}] \tag{2}$$

$\boldsymbol{D}_{\mathrm{DPV}}$, $\boldsymbol{D}_{\mathrm{LSV}}$, $\boldsymbol{D}_{\mathrm{CV}}$, $\boldsymbol{D}_{\mathrm{UVVis}}$ and $\boldsymbol{D}_{\mathrm{F}}$ contain the data recorded by DPV, LSV, CV, UVVis and F as instrumental techniques. $\boldsymbol{C}^{\mathrm{CBG}}$ and $\boldsymbol{C}^{\mathrm{HSA}}$ contain the concentration profiles.

Evolving Factor Analysis (EFA) is able to provide an initial estimation of changing concentration of the species during the experiment [23–26], and during ALS optimization some constraints are used to facilitate the finding of representative contributions and to obtain chemically meaningful results [26]. The lack of fit (*lof*) is a criterion to examine the goodness of fit of the model which can be calculated according to the following equation [27]:

$$lof\ (\%) = 100\sqrt{\frac{\sum_{i,j} e_{i,j}^2}{\sum_{i,j} d_{i,j}^2}} \tag{3}$$

where d_{ij} and e_{ij} refer to the elements of the raw data and their corresponding residuals, respectively.

The solutions which are used by MCR are not unique and may have some rotational and intensity ambiguities and matrix augmentation can tackle this problem. Furthermore, this method can be useful to overcome small signal shifts observed in the data as well. Therefore, an augmented data matrix was built and submitted for the resolution by MCR-ALS. However, because of combining different types of instrumental data, following considerations must not be neglected:

1. Because of the more intensity of the voltammetric data than spectroscopic data, all the submatrices must be normalized by dividing them by their maximum values.
2. Here, the concept of component is more complicated because of having different types of instrumental data. From spectroscopic

point of view, a component is a pure chemical species in solution [28,29], but for electrochemists a component is more complicated because from electrochemical point of view, a component not only associated to a single electrochemical process, but also is associated with the other phenomena such as adsorption or capacitive currents [30,31].

3. For combining voltammetric and spectroscopic matrices to build an augmented data matrix, all the matrices must have a same number of rows and columns and a same distribution of the species during the experiments. Achieving this goal needs a same total concentration in all titrations for both of CBG and HSA. Achieve to this condition is impossible, because for voltammetric experiments higher concentrations are needed than spectroscopic ones. To tackle this problem, all the voltammetric and spectroscopic experiments were performed at different total concentrations but with the same values of ratio.

3. Results and discussion

3.1. Voltammetric studies of CBG-HSA interactions

3.1.1. CV studies

CV as a powerful electroanalytical technique has been frequently used to investigate protein-small molecule interactions [32]. Therefore, in this section, we have use it for investigation of CBG-HSA interactions. To achieve this goal, to a solution containing a constant concentration of CBG (1.0×10^{-4} M) HSA was added in the range of 0–1.0×10^{-4} M and the results are shown in Fig. 3A. The CV response of CBG can be seen as the first CV of Fig. 3A, and by adding HSA to CBG, the peak intensity and peak potential were decreased and increased, respectively, which confirmed the interactions of CBG with HSA [33]. The mentioned phenomena also confirmed interactions of CBG with hydrophobic region of the HSA cavity. E_p and $E_{p/2}$ values of the CV response of the CBG at the GCE surface were 170 and 140 mV, respectively. According to $|E_p - E_{p/2}| = 47.7/\alpha n$ [34] which is related to an irreversible oxidation, where n is the electron transfer number and $\alpha = 0.5$ [35], n was calculated to be 3.18 i.e. ~ 3.

Immobilization of a biological macromolecule such as HSA at the GCE surface can give us some information about the type of interactions of a small molecule with HSA [36,37]. Therefore, the CV response of CBG at bare GCE (curve *a*) and HSA/GCE (curve *b*) were recorded and can be seen in Fig. 3B. As can be seen, the CV response of the CBG at the surface of HSA/GCE was appeared in more positive potentials which confirmed that the CBG-HSA interactions were occurred by hydrophobic forces [36].

The binding constant of CBG-HSA complex was computed with the help of CV by recording the CVs of different concentrations of CBG at the surface of HSA/GCE (not shown). The intensity of the CVs was increased with increasing concentration of CBG (C_{CBG}) and reached to saturation values. According to Eq. (4) [38], where I, I_{max}, and K_b are the peak current, maximum peak current and the binding constant of CBG at the surface of HSA/GCE, respectively, the K_b value was

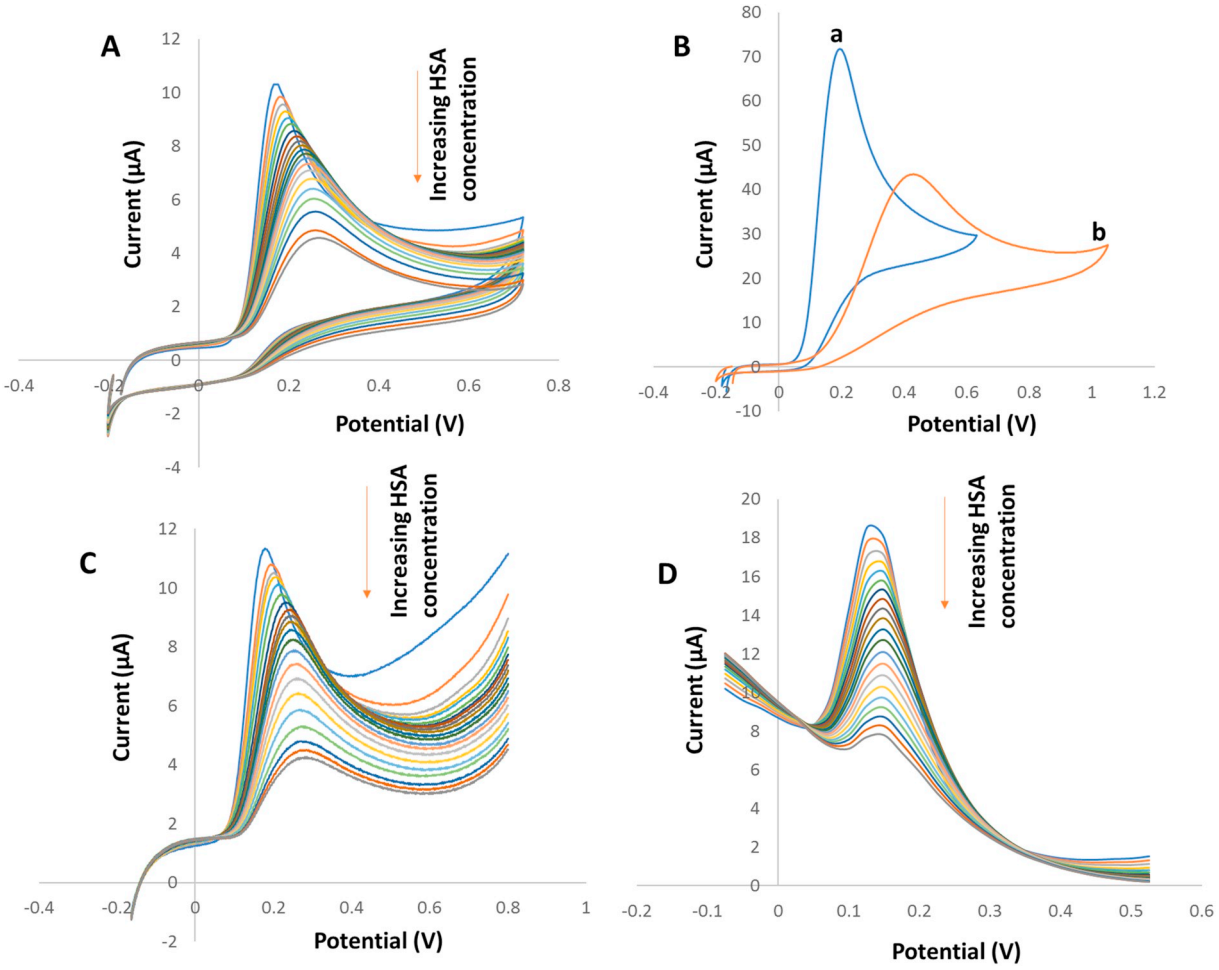

Fig. 3. (A) The CV responses of 1.0×10^{-4} M CBG in the presence of increasing concentration of HSA ranging in 0–1.0×10^{-4} M, (B) the CV responses of 5.0×10^{-4} M CBG at the surface of bare GCE (curve a) and HSA/GCE (curve b), (C) the LSV responses of 1.0×10^{-4} M CBG in the presence of increasing concentration of HSA ranging in 0–1.0×10^{-4} M and (D) the DPV responses of 1.0×10^{-5} M CBG in the presence of increasing concentration of HSA ranging in 0–1.0×10^{-5} M.

calculated to be $4.11 \times 10^5\,mol^{-1}\,L$ by the regression of C_{CBG}/I on C_{CBG}.

$$C_{CBG}/I = (1/K_b I_{max}) + (C_{CBG}/I_{max}) \quad (4)$$

3.1.2. LSV and DPV studies

The LSVs and DPVs of CBG at the surface of GCE upon increasing HSA concentration were recorded in the PBS (0.05 M, pH 7.4) and are presented in Fig. 3C and D, respectively. As can be seen, by the addition of HSA the CVs of CBG were decreased and shifted to more positive potentials which were related to the CBG-HSA interactions. During interaction of CBG with HSA, the equilibrium concentration of CBG is decreased due to locating of the CBG in the HSA structure. Competitive adsorption at the GCE surface is another phenomenon which may be occurred. When a low concentration of a biological macromolecule such as HSA is interacted with a small molecule, only a low area of the electrode surface (10%) is covered which confirms a low competitive adsorption of the small molecules at the surface of the electrode [39,40]. Therefore, the changes observed in the CV response of CBG in the presence of increasing concentration of HSA were related to interaction of CBG with HSA and complex formation. But multivariate analysis of the data in next sections will help us to have a better judgment about CBG-HSA interactions.

3.2. Spectroscopic studies of CBG-HSA interactions

3.2.1. Spectrofluorimetry

The fluorescence emission spectra of 2.0×10^{-7} M HSA ($\lambda_{ex} = 280$ nm) upon increasing concentration of CBG, 0.0–1.0×10^{-6} M, were recorded at three different temperatures (i.e., 298.15, 304.15 and 310.15 K) and one of them (298.15 K) is shown in Fig. 4A. As can be seen, the intensity of the emission of HSA was decreased with increasing CBG concentration. The intrinsic fluorescence HSA is related to its Trp-214 and by the interaction of a small molecule with HSA, its fluorescence intensity is decreased [41]. Fluorescence quenching can be occurred by different molecular interactions such as energy transfer, molecular rearrangements, excited state reactions, ground state complex formation, and collisional quenching. Usually, quenching is occurred by dynamic collision and static quenching (complex formation) and to declare the mechanism of quenching, Stern-Volmer equation is used [42]:

$$F_0/F = 1 + K_{SV}[Q] \quad (5)$$

where F_0 and F are the steady-state fluorescence intensities in the absence and presence of CBG as the quencher, respectively, and K_{SV} is the Stern-Volmer quenching constant. According to Eq. (5), the results of the regression of F_0/F on concentrations of CBG are presented in Table S2. As can be seen, the K_{SV} values are decreasing with increasing temperature suggesting a static quenching (complex formation) for quenching of HSA by CBG.

3.2.2. Site selectivity of binding of CBG to HSA

There are two sites in HSA including site I (hydrophobic sub-domain IIA) [43] and Sudlow's sites II (sub-domain IIIA) [44] which enable small molecules for binding with HSA. For identifying the location of binding of CBG with HSA, we performed two competitive experiments with two site markers including Wr (marker of site I) and Ip (marker of site II). To perform these competitive experiments, to a solution containing CBG and HSA where CBG concentration (2.0×10^{-7} M) was four times higher than that of HSA (5.0×10^{-8} M) Wr or Ip was added in the range of 0.0–2.0×10^{-7} M. Subsequently, $(F_1/F_2) \times 100$ (F_1 and F_2 refer to the fluorescence intensity in the absence and presence of Wr or Ip as site marker, respectively) was plotted against [Site Marker]/[HSA] and the results are shown in Fig. 4B. The variations observed by the addition of site marker to the mixture of CBG and helped us to distinguish the binding location of CBG on HSA. The results showed that $(F_1/F_2) \times 100$ was decreased by the addition of Wr to the HSA-CBG solution (Fig. 4B, curve *a*) which confirmed that the binding of CBG with HSA was affected by the addition of Wr. By doing the same procedure but in the presence of Ip, the $(F_1/F_2) \times 100$ was not affected (Fig. 4B, curve *b*) which confirmed that the binding of CBG with HSA was not affected by Ip. The results obtained from the experiments mentioned above confirmed that Wr is competed with CBG while Ip does not. Therefore, the binding site of CBG was located in sub-domain IIA of HSA.

3.2.3. Spectrophotometry

Interaction of CBG with HSA was also investigated spectrophotometrically by the titration of 5.0×10^{-5} M HSA with increasing concentration of CBG in the range of 0.0–2.5×10^{-4} M and the spectra are shown in Fig. 4C. As can be seen, the position and intensity of the absorbance peak of HSA at 280 nm were affected by the addition of CBG which confirm the interactions of CBG with HSA.

3.2.4. Energy transfer from HSA to CBG and measurement of the binding distance

Fluorescence energy transfer (FRET) as a general spectroscopic method is usually used to determine the molecular distance in biological systems [45]. The efficiency (E, Eq. (6)) of FRET is affected by some factors such as the inverse sixth power of the distance between donor and acceptor (r) that should be be within 2–8 nm which is also called Forster distance [46], Forster radius (R_0, Eq. (7)), overlapping of the emission of the donor with the absorption of the acceptor and orientation of the transition dipole of the donor.

$$E = 1 - \frac{F}{F_0} = \frac{R_0^6}{(R_0^6 + r^6)} \quad (6)$$

$$R_0^6 = 8.8 \times 10^{-25} k^2 n^{-4} J \Phi \quad (7)$$

n and k^2 are refractive index of the medium and spatial factor of orientation, respectively. Φ and J fluorescence are quantum yield of the donor and the overlap integral of the fluorescence emission spectrum for the donor and the absorption spectrum of the acceptor, respectively. The J can be defined according to the following equation:

$$J = \frac{\int_0^\infty F(\lambda)\varepsilon(\lambda)\lambda^4 d\lambda}{\int_0^\infty F(\lambda) d\lambda} \quad (8)$$

where $F(\lambda)$ is the fluorescence intensity of the donor and ε is molar absorption coefficient of the acceptor. Values of k^2, n and Φ are 2/3, 1.336 and 0.118, respectively, which can be found elsewhere [47]. According to the values mentioned above, J, R_0, E and r were calculated to be $5.14 \times 10^{-14}\,cm^3\,M^{-1}$, 3.22 nm, 0.01 and 3.21 nm, respectively. As can be seen, r is fallen in Forster distance which confirms that the energy transfer can be ocurred from HSA to CBG [48].

3.3. Combination of voltammetric and spectroscopic data

In this section of our study, we have built an augmented data matrix by the combination of voltammetric and spectroscopic data which was used as the input of MCR-ALS. In next section, we will justify the outputs of MCR-ALS.

3.3.1. Justification of the MCR-ALS results

In order to obtain more information about interactions of CBG with HSA, the augmented data matrix was analysed by MCR-ALS. The outputs of MCR-ALS can help us to detect any HSA-CBG_m complex and to obtain relative concentrations of the various species. To build the augmented data matrix, individual data matrices including DPV ($\boldsymbol{D}_{DPV}^{CBG}$, Fig. 3D, $\boldsymbol{D}_{DPV}^{HSA}$, Fig. 4D), LSV ($\boldsymbol{D}_{LSV}^{CBG}$, Fig. 3C, $\boldsymbol{D}_{LSV}^{HSA}$, Fig. 5A), CV ($\boldsymbol{D}_{CV}^{CBG}$, Fig. 3A, $\boldsymbol{D}_{CV}^{HSA}$, Fig. 5B), UVVis ($\boldsymbol{D}_{UVVis}^{CBG}$, Fig. 5C, $\boldsymbol{D}_{UVVis}^{HSA}$, Fig. 4C) and F ($\boldsymbol{D}_{F}^{HSA}$, Fig. 4A, $\boldsymbol{D}_{F}^{CBG}$, Fig. 5D) were

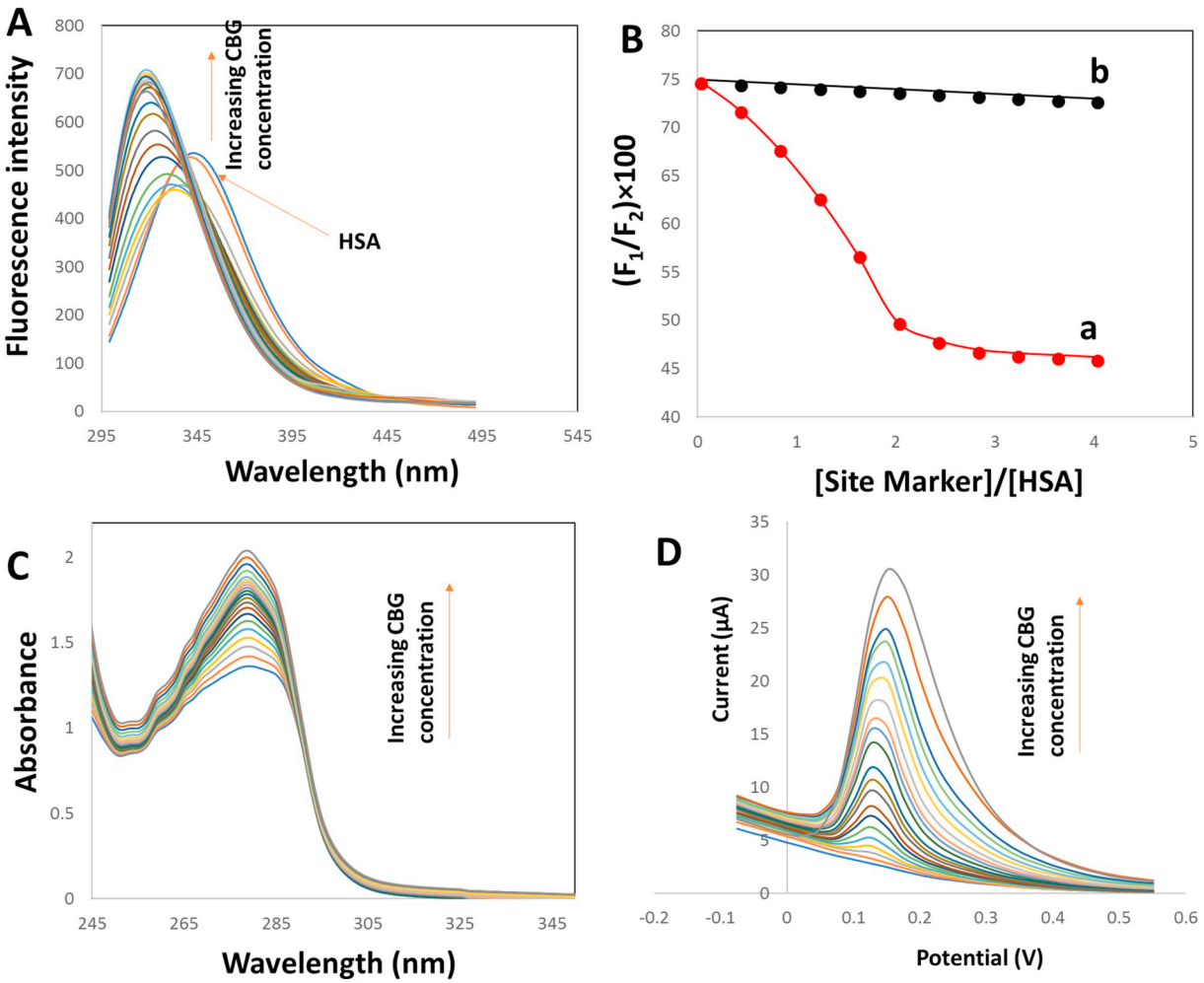

Fig. 4. (A) Spectrofluorimetric data recorded for 2.0×10^{-7} M HSA (λ_{ex} = 280 nm) in the presence of increasing concentration of CBG in the range of 0–1.0×10^{-6} M, (B) effects of Wr (curve a) and Ip (curve b) on the fluorescence emission of HSA-CBG, (C) UVVis absorption spectra of 5.0×10^{-5} M HSA in the presence of increasing concentration of CBG in the range of 0–2.5×10^{-4} M and (D) the DPV responses of 1.0×10^{-5} M HSA in the presence of increasing concentration of CBG in the range of 0–5.0×10^{-5} M.

column- and row-wise augmented.

The first attempt was included using singular value decomposition (SVD) for determination of the number of species and after applying it to the augmented data matrix, three main components were detected which may be related to free CBG, free HSA and one HSA-CBG_m complex species. The second attempt was including application of the EFA to obtain an initial estimate of the concentration profiles of the involved species. The EFA can work with a full rank data matrix and its application to a rank-deficient data matrix cannot give us useful information. This problem can be tackled by matrix augmentation [49]. In MCR-ALS because of using constraints more reliable results could be obtained. In our work, because of the presence of the CV data which contain negative values in their reverse direction, the non-negativity constraint was only applied to the concentration profiles and application of the closure constraint to the matrices obtained at different concentration levels was not possible.

With the conditions mentioned above, the iterative ALS was used to optimize the results of MCR and the *lof* was used to evaluate the goodness of the fitting procedure. Here, a value of 4.88% was found as the lowest value for *lof* which confirmed an acceptable fitting procedure by MCR-ALS. The results of MCR-ALS are shown in Figs. 6 and 7. Fig. 6A and B are related to the concentration profiles of the species. According to Fig. 6A, by the addition of HSA to CBG, CBG concentration is decreased and a new complex is forming. By casting a look on the variation of the concentration of the complex specie, it can be found that its concentration is sharply increased at [HSA]/[CBG]~0.5 which confirms forming a HSA-CBG_2 complex specie. Fig. 6B shows that the at [CBG]/[HSA]~2 concentration of the complex is equilibrated and concentrations of HSA and CBG are vigorously decreased and increased, respectively. The results obtained from the analysis of the details of Fig. 6B confirms complex formation is mainly occurred at [CBG]/[HSA] ~2 which also confirms that the complex specie is HSA-CBG_2. The pure voltammetric and spectral profiles obtained by MCR-ALS are shown in Fig. 7A-E which can help us to obtain new information about the nature of the species. The results show that HSA is electro-inactive with its original structure while the complex specie is electroactive. By locating the CBG within the HSA structure, the protein will be unfolded which cause tryptophan and tyrosine residues to be accessible for oxidation at the electrode surface. Therefore, the complex will be electroactive. A plot with coincided experimental and theoretical points (Fig. 7F) was obtained for the fitting procedure which confirms the existence of a high-quality fitting procedure.

3.3.2. Verification of the existence of ambiguities in MCR-ALS results by MCR-BANDS

As mentioned in previous sections, application of constraints can help us to obtain reliable and meaningful results for MCR-ALS which is an important advantage for MCR-ALS [50]. However, sometimes, a band of feasible solutions are applied instead of a unique solution which may cause the existence of some ambiguities in the results [51].

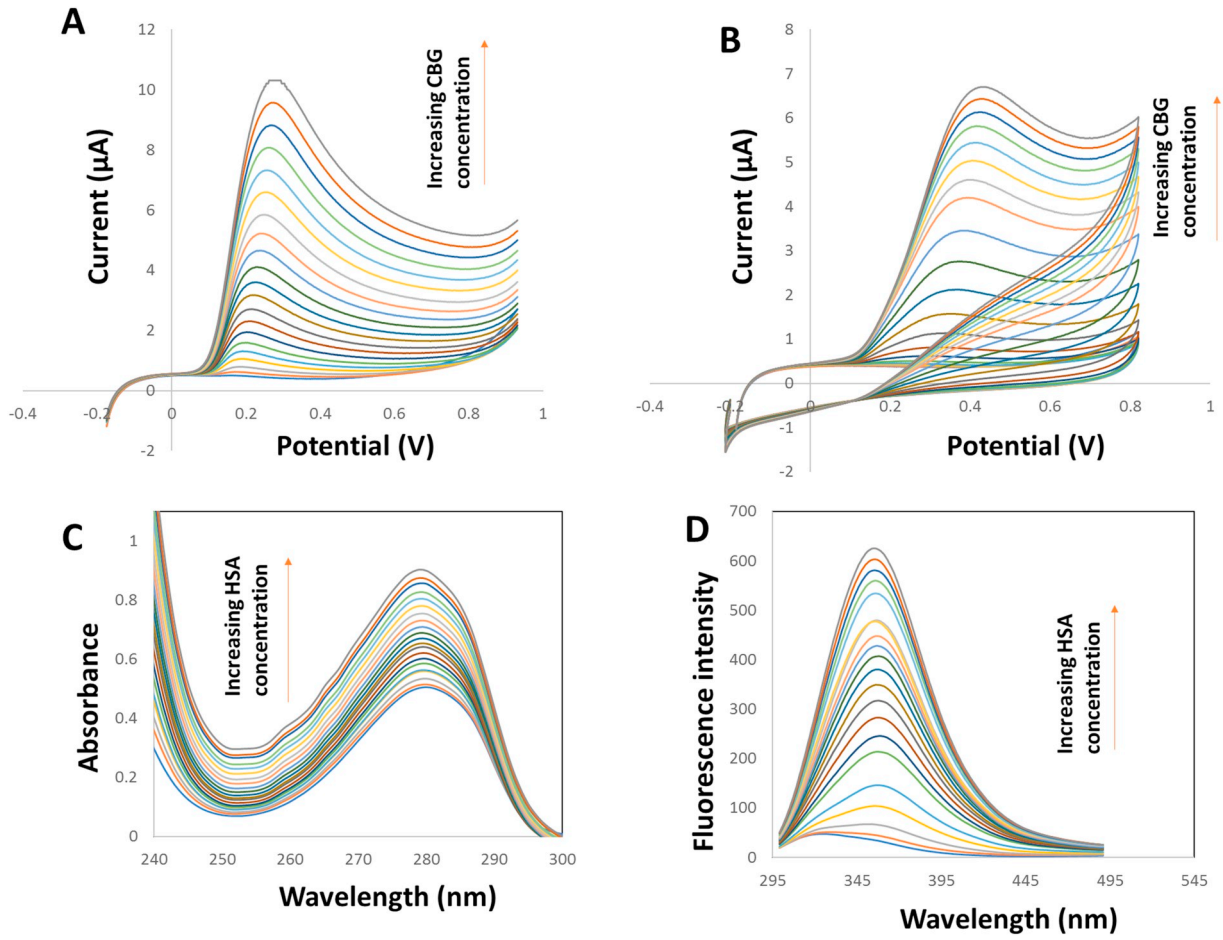

Fig. 5. (A) The LSV responses of 1.0×10^{-4} M HSA in the presence of increasing concentration of CBG in the range of 0–5.0×10^{-4} M, (B) the CV responses of 1.0×10^{-4} M HSA in the presence of increasing concentration of CBG in the range of 0–5.0×10^{-4} M, (C) UVVis absorption spectra of 1.0×10^{-4} M CBG in the presence of increasing concentration of CBG in the range of 0–1.0×10^{-4} M CBG and (D) fluorescence emission spectra of 1.0×10^{-7} M CBG in the presence of increasing concentration of HSA in the range 0–1.0×10^{-7} M.

Therefore, verification of the results of MCR-ALS to identify the presence of ambiguities is necessary and MCR-BANDS has been developed as an efficient chemometric tool to compute the maximum and minimum of the relative contribution of the components for estimating the feasible solutions which can help us to estimate the extent of rotational ambiguity [50,52,53].

Here, the MCR-BANDS with the same constraints used for MCR-ALS was applied to results of MCR-ALS and the maximum relative contribution function (f^{max}) and minimum relative contribution function (f^{min}) for each contributing species were calculated to be HSA ($f^{max} = 0.545$ and $f^{min} = 0.545$), CBG ($f^{max} = 0.398$ and $f^{min} = 0.398$) and HSA-CBG_2 ($f^{max} = 0.511$ and $f^{min} = 0.511$). Fortunately, for all the species there was no difference between the f^{max} and f^{min} which confirmed that there wasn't any rotational ambiguity [50].

3.4. Hard-modeling of experimental data

For decomposition of the data matrix ***D*** according to Eq. (1) by a

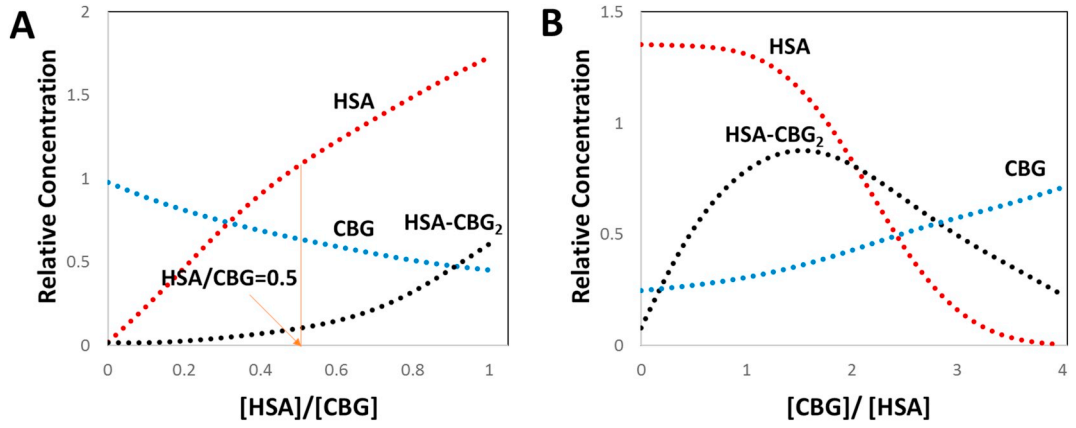

Fig. 6. (A) and (B) concentration profiles of the species involved extracted as the outputs of MCR-ALS after analyzing the augmented data matrix.

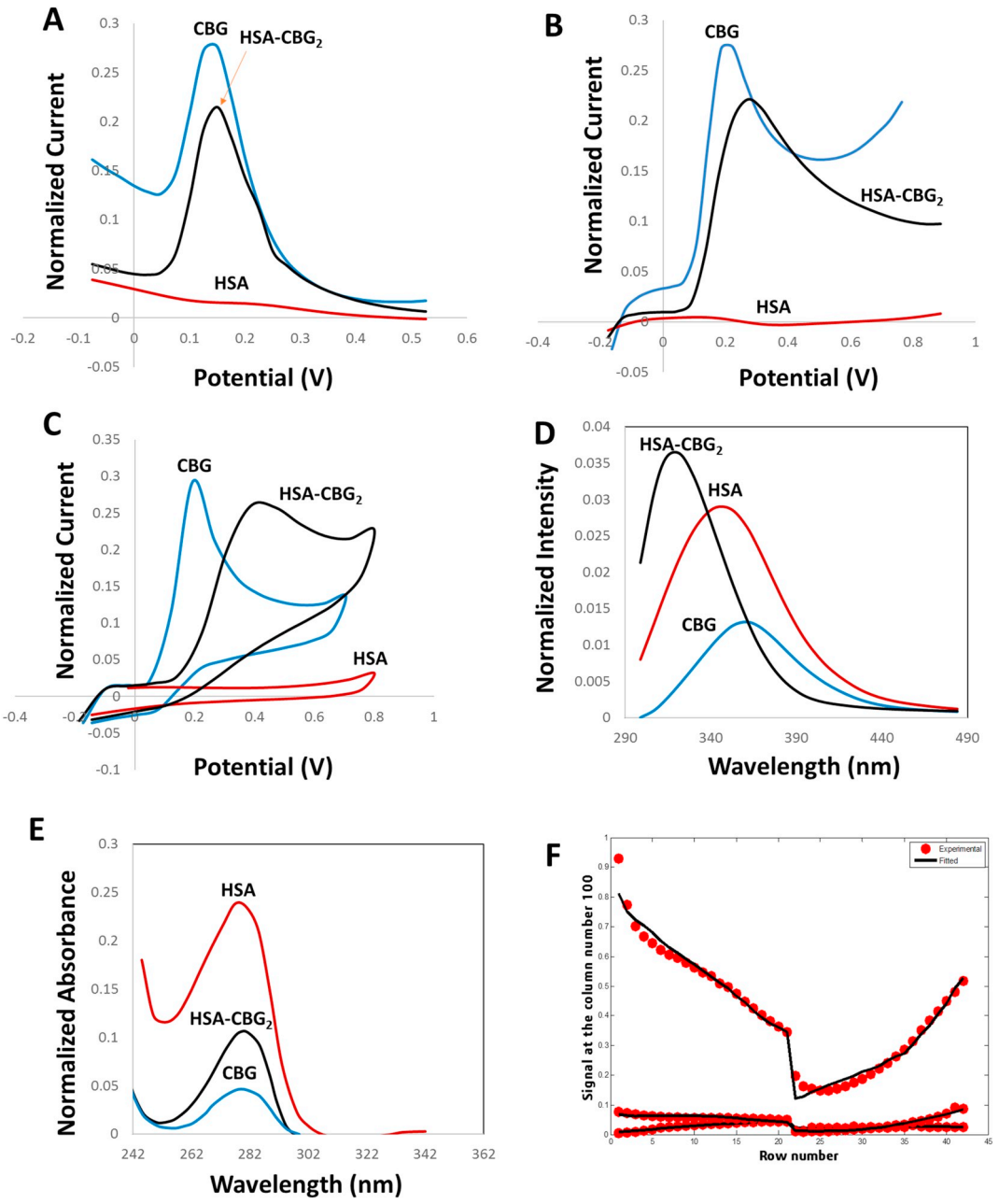

Fig. 7. (A)-(E) extracted signals of different species involved in DPV, LSV, CV, F and UVVis experiments, respectively, and (F) plotting experimental (points) and calculated data (line) as a criterion for evaluation of the goodness of the fitting procedure.

hard-modeling algorithm, a model must be defined which contains stoichiometry of the species involved and an estimation of the binding constant. The defined model is used as an input for the hard-modeling algorithm to obtain an estimation for the concentration profiles (***C***) and then, least squares fitting is applied to resolve the pure spectra ($\boldsymbol{S}^{T}$) by the best matching of ***C*** and ***D***. The differences between the input data (***D***) and the reproduced data matrix by the algorithm are collected into a residual matrix (***E***). The hard-modeling algorithm repeats the optimization process until a suitable level of residuals is obtained. For obtaining more information about details of the hard-modeling approach, the reader is referred to read Ref. [54].

In the present work, EQUISPEC as a hard-modeling algorithm was used to calculate the binding constants and also was used as a criterion for verifying the results of Section 3.1.1. The results are presented in Table 1. As can be seen, there is a good agreement between the results of EQUISPEC and those of Section 3.1.1.

Table 1
Results of calculating binding constant by EQUISPEC.

Analysed matrix	K_b
	HSA-CBG_2
$[\boldsymbol{D}_{DPV}{}^{CBG}\boldsymbol{D}_{LSV}{}^{CBG}\boldsymbol{D}_{CV}{}^{CBG}\boldsymbol{D}_{F}{}^{CBG}\boldsymbol{D}_{UVVis}{}^{CBG}]$	4.31×10^5
$[\boldsymbol{D}_{DPV}{}^{HSA}\boldsymbol{D}_{LSV}{}^{HSA}\boldsymbol{D}_{CV}{}^{HSA}\boldsymbol{D}_{F}{}^{HSA}\boldsymbol{D}_{UVVis}{}^{HSA}]$	4.52×10^5
$\begin{bmatrix} \boldsymbol{D}_{DPV}^{CBG}\boldsymbol{D}_{LSV}^{CBG}\boldsymbol{D}_{CV}^{CBG}\boldsymbol{D}_{F}^{CBG}\boldsymbol{D}_{UVVis}^{CBG} \\ \boldsymbol{D}_{DPV}^{HSA}\boldsymbol{D}_{LSV}^{HSA}\boldsymbol{D}_{CV}^{HSA}\boldsymbol{D}_{F}^{HSA}\boldsymbol{D}_{UVVis}^{HSA} \end{bmatrix}$	4.28×10^5

3.5. Molecular docking

In this section, the MVD software was used to build a computer generated CBG-HSA interaction and the results are shown in Fig. 8A-C. After docking of CBG to HSA, the binding sites were detected as Trp

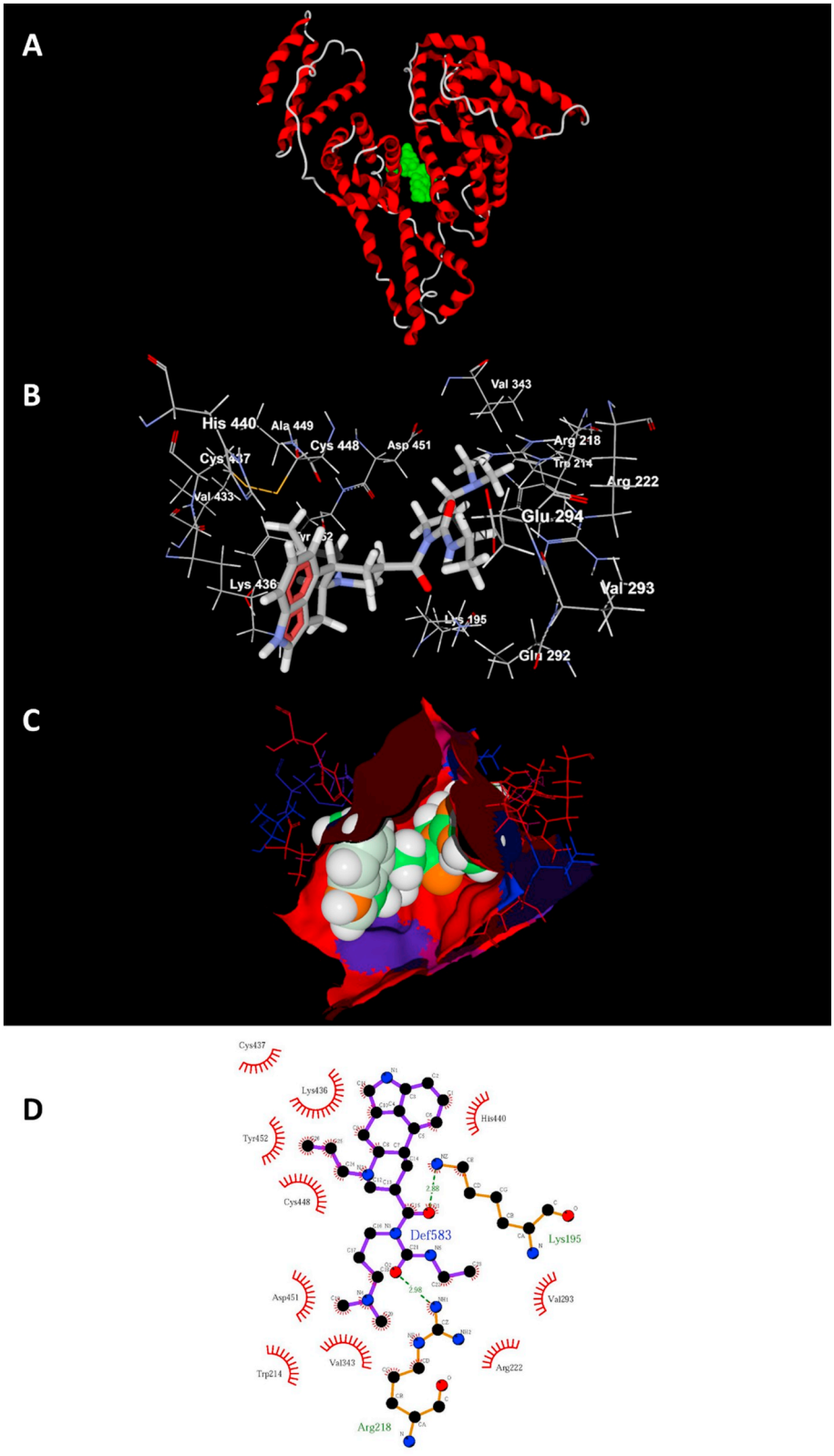

Fig. 8. Results of docking of CBG to HSA presented by: (A) secondary structure view, (B) pose organizer view and (C) hydrophobicity view. (D) CBG-HSA interactions presented by LigPlot program.

214, Val 343, Arg 218, Arg 222, Asp 451, Lys 195, Val 293, Glu 292, Glu 294, Ala 449, Cys 448, Tyr 452, Val 433, Cys 437, His 440 and Lys 436. The ΔG for binding of CBG to HSA was calculated to be $-32.15\ \mathrm{kJ\ mol^{-1}}$. As can be seen, CBG has been bound to sub-domain IIA of HSA which confirmed the results of experimental sections. The LIGPLOT program was used to detect the hydrogen binding hydrophobic interactions between CBG and HSA and the results are shown in Fig. 8D. By the analysis of the LIGPLOT results, there are two hydrogen bonds between CBG and Lys 195 and CBG and Arg 218, and hydrophobic interactions were observed between CBG and Cys 437, Lys 436,

Tyr 452, His 440, Cys 448, Asp 451, Val 293, Trp 214, Val 343 and Arg 222 from HSA.

3.6. Analytical characterizations

In this section, we are going to introduce a novel electroanalytical methodology for determination of HSA based on CBG-HSA interactions. Due to much higher sensitivity of amperometric methods than voltammetric techniques, electrochemical sensing of HSA was performed by amperometric methods. Another action which was performed for increasing the sensitivity of the developed electroanalytical methodology was included modification of the bare GCE which has been suggested by the previous works [55–59]. Here, the bare GCE was modified with MWCNTs-IL.

3.6.1. Amperometric measurements

To develop an electroanalytical methodology for determination of electro-inactive HSA, two different amperometric experiments in the presence and absence of HSA were performed in a gently stirred (1000 rpm) PBS (0.05 M, pH 7.4) as supporting electrolyte. To perform the first amperometric experiment, different concentrations of CBG in the range of 5–90 μM were injected into the electrochemical cell where potential was fixed at 0.09 V and its *i-t* curve can be seen in Fig. 9A. The second amperometric experiment was the same as the first one but in the presence of increasing concentration of HSA in the range of 1–40 μM and its *i-t* curve can be seen in in Fig. 9B. For building a calibration curve for electrochemical sensing of HSA, $\Delta i = i\text{-}i^*$ values were regressed on HSA concentrations which can be seen in Fig. 9C. Two linear ranges of 1–9.5 μM and 9.5–40 μM were observed for the biosensing of HSA. The sensitivity and limit of detection of the sensor were calculated to be 6.47 μA μM^{-1} and 0.6 μM (according to $3SD/m$, where *SD* is the standard deviation of the intercept and *m* is the slope of the calibration curve), respectively.

3.6.2. Interference study

Amperometric responses of the MWCNTs-IL/GCE to HSA (10 μM) in the presence of 100-fold interfering species including (a) cysteine, (b) tyrosine, (c) histidine, (d) valine, (e) methionine, (f) proline, (g) phenylalanine, (h) egg albumin, (i) chloramphenicol, (j) amoxicillin, (k) vitamin C and (l) vitamin B12 is shown in Fig. 9D. The results show that the sensor had a selective response to HSA even in the presence of interfering species.

3.6.3. Stability, repeatability, and reproducibility

Stability is an important characteristic for a sensor which must be verified and reported. Therefore, the sensor was applied to weekly determination of 10 μM HSA during six weeks. Results confirmed that the sensor was able to retain 96.1% of its original response which was a good guarantee for the stability of the sensor. The repeatability of the sensor was also examined by the application of the sensor to determination of 10 μM HSA for ten times during a day and the results confirmed a good repeatability for the sensor whose relative standard deviation (RSD) was 2.41%. For verification of the reproducibility of the sensor, six sensors were constructed and applied to the determination of

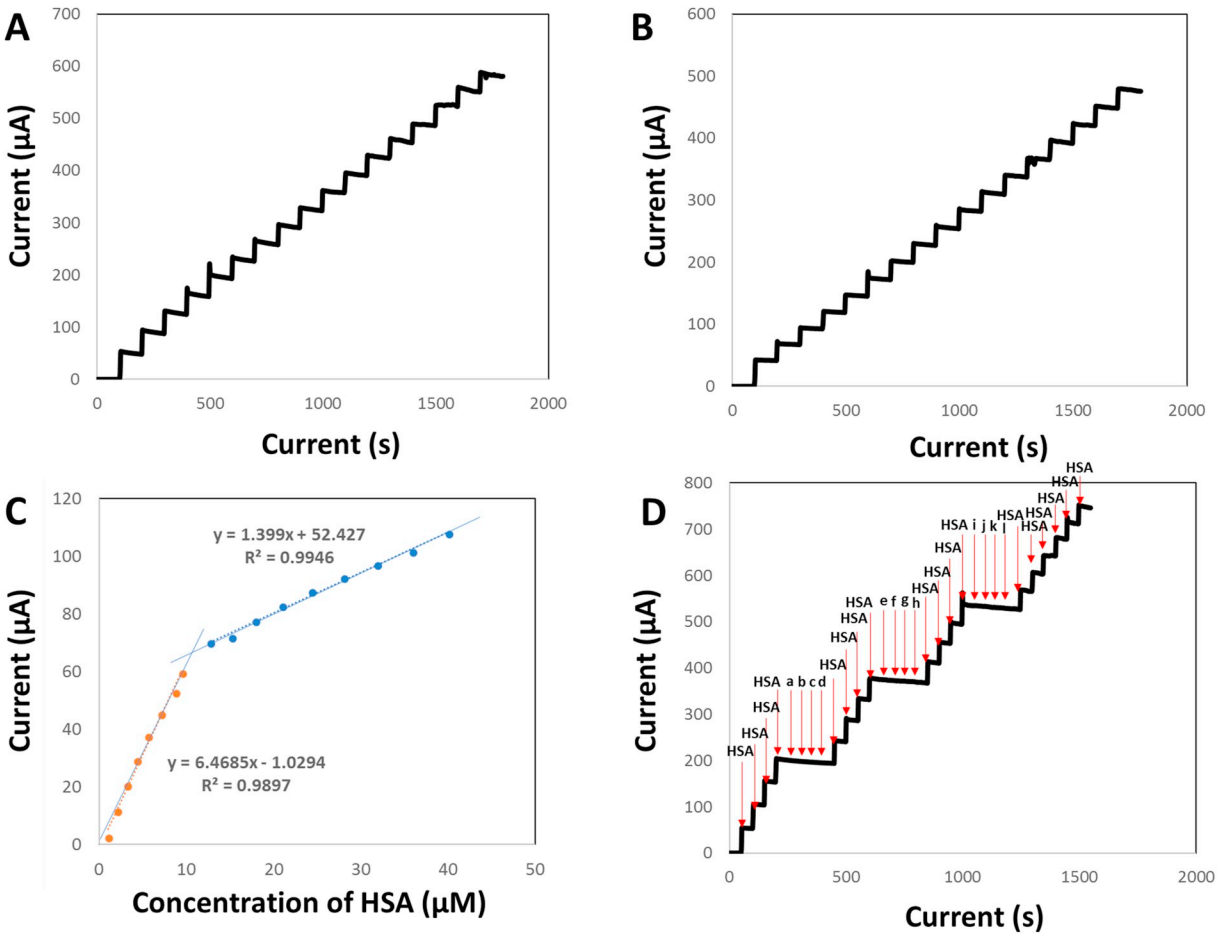

Fig. 9. (A) Amperometric responses recorded by MWCNTs-IL/GCE upon increasing concentration of CBG, (B) same as (A) but, in the presence of increasing concentration of HSA, (C) regression of $\Delta i = i\text{-}i^*$ on HAS concentrations and (D) amperometric responses of the sensor to HSA and in the presence of interfering species: (a) cysteine, (b) tyrosine, (c) histidine, (d) valine, (e) methionine, (f) proline, (g) phenylalanine, (h) egg albumin, (i) chloramphenicol, (j) amoxicillin, (k) vitamin C and (l) vitamin B12.

Table 2
Results of the analysis of human serum samples by the reference method and proposed method in this study.

Sample	Found by the proposed method in this study (n = 4)	Found by the reference method (n = 4)
Serum 1	7.11 (± 0.05) × 10^{-4} M	7.21 (± 0.03) × 10^{-4} M
Serum 2	6.88 (± 0.03) × 10^{-4} M	6.96 (± 0.04) × 10^{-4} M
Serum 3	7.28 (± 0.02) × 10^{-4} M	7.31 (± 0.05) × 10^{-4} M

10 μM HSA. A suitable value of 3.01% was found for RSD which confirmed reproducibility of the sensor response.

3.6.4. Validation of the developed methodology

For verification of the ability of the sensor for HSA determination in human serum samples, its results were compared with the results of a medical diagnostic laboratory which used capillary electrophoresis as the reference method for the analysis of real samples. The results of the two methods are collected in Table 2 and as can be seen, there is an acceptable agreement between the two methods.

4. Conclusions

In the present study, interactions of CBG with HSA were investigated by experimental and computational methods which helped us to have a deep inside to CBG-HSA interactions. Firstly, electrochemical and spectroscopic data were separately analysed to obtain some information and then, by the combination of the data into an augmented data matrix and analyzing by MCR-ALS new information was extracted. The results of the multivariate analyses gave new information about the number of species involved and their stoichiometry and their electrochemical nature. The CBG was also docked with HSA by molecular docking methods which enabled us to obtain new information about the location of the CBG at HSA and type of its interaction with HSA. The results obtained from experimental and computational sections were compatible. Finally, a novel, fast, simple and low-cost electroanalytical method was developed based on CBG-HSA interactions for determination of electro-inactive HSA.

Acknowledgements

Hereby, we acknowledge the financial supports of this project by Research Council of Kermanshah University of Medical Sciences.

Appendix A. Supplementary data

Supplementary data to this article can be found online at https://doi.org/10.1016/j.sbsr.2019.100297.

References

[1] https://www.drugbank.ca/drugs/DB00248.
[2] M.B. Gholivand, A.R. Jalalvand, H.C. Goicoechea, M. Omidi, Investigation of interaction of nuclear fast red with human serum albumin by experimental and computational approaches, Spectrochim. Acta A 115 (2013) 516–527.
[3] M.B. Gholivand, A.R. Jalalvand, H.C. Goicoechea, R. Gargallo, T. Skov, Chemometrics: an important tool for monitoring interactions of vitamin B7 with bovine serum albumin with the aim of developing an efficient biosensing system for the analysis of protein, Talanta 132 (2015) 354–365.
[4] M.B. Gholivand, A.R. Jalalvand, H.C. Goicoechea, T. Skov, Fabrication of an ultrasensitive impedimetric buprenorphine hydrochloride biosensor from computational and experimental angles, Talanta 124 (2014) 27–35.
[5] M.B. Gholivand, A.R. Jalalvand, H.C. Goicoechea, Developing a novel computationally designed impedimetric pregabalin biosensor, Electrochim. Acta 133 (2014) 123–131.
[6] M.B. Gholivand, A.R. Jalalvand, G. Paimard, H.C. Goicoechea, T. Skov, R. Farhadi, S. Ghobadi, N. Moradi, V. Nasirian, Fabrication of a novel naltrexone biosensor based on a computationally engineered nanobiocomposite, Int. J. Biol. Macromol. 70 (2014) 596–605.
[7] A.R. Jalalvand, S. Ghobadi, H.C. Goicoechea, H.W. Gu, E. Sanchooli, Investigation of interactions of Comtan with human serum albumin by mathematically modeled voltammetric data: a study from bio-interaction to biosensing, Bioelectrochemistry 123 (2018) 162–172.
[8] G. Mohammadi, E. Faramarzi, M. Mahmoudi, S. Ghobadi, A.R. Ghiasvand, H.C. Goicoechea, A.R. Jalalvand, Chemometrics-assisted investigation of interactions of Tasmar withhuman serum albumin at a glassy carbon disk: application toelectrochemical biosensing of electro-inactive serum albumin, J. Pharm. Biomed. Anal. 156 (2018) 23–35.
[9] Y.Y. Yue, X.G. Chen, J. Qin, X.J. Yao, Characterization of the mangiferin–human serum albumin complex by spectroscopic and molecular modeling approaches, J. Pharm. Biomed. Anal. 49 (2009) 753–759.
[10] J.S. Mandeville, E. Froehlich, H.A. Tajmir-Riahi, Study of curcumin and genistein interactions with human serum albumin, J. Pharm. Biomed. Anal. 49 (2009) 468–474.
[11] H.X. Luo, Y. Du, Z.X. Guo, Electrochemistry of N-n-undecyl-N′-(sodium-p-aminobenzenesulfonate) thiourea and its interaction with bovine serum albumin, Bioelectrochemistry 74 (2009) 232–235.
[12] Q.H. Lu, C.D. Ba, D.Y. Chen, Investigating noncovalent interactions of rutin – serum albumin by capillary electrophoresis – frontal analysis, J. Pharm. Biomed. Anal. 47 (2008) 888–891.
[13] C. Bertucci, V. Andrisano, R. Gotti, V. Cavrini, Use of an immobilised human serum albumin HPLC column as a probe of drug–protein interactions: the reversible binding of valproate, J. Chromatogr. B 768 (2002) 147–155.
[14] B. Bojko, A. Sulkowska, M. Maciazek-Jurczyk, J. Rownicka, W.W. Sulkowski, Investigations of acetaminophen binding to bovine serum albumin in the presence of fatty acid: Fluorescence and 1H NMR studies, J. Mol. Struct. 924-926 (2009) 332–337.
[15] Y.N. Ni, S.S. Wang, S. Kokot, Spectrometric study of the interaction between Alpinetin and bovine serum albumin using chemometrics approaches, Anal. Chim. Acta 663 (2010) 139–146.
[16] Y.N. Ni, G.L. Liu, S. Kokot, Fluorescence spectrometric study on the interactions of Isoprocarb and sodium 2-isopropylphenate with bovine serum albumin, Talanta 76 (2008) 513–521.
[17] A.C. Wallace, R.A. Laskowski, J.M. Thornton, LIGPLOT: a program to generate schematic diagrams of protein-ligand interactions, Protein Eng. 8 (1995) 127–134.
[18] http://www.ub.es/gesq/mcr/mcr.htm.
[19] M.B. Gholivand, A.R. Jalalvand, H.C. Goicoechea, Multivariate analysis for resolving interactions of carbidopa with dsDNA at a fullerene-C60/GCE, Int. J. Biol. Macromol. 69 (2014) 369–381.
[20] A.R. Jalalvand, H.C. Goicoechea, D.N. Rutledge, Applications and challenges of multi-way calibration in electrochemical analysis, Trends Anal. Chem. 87 (2017) 32–48.
[21] A.R. Jalalvand, H.C. Goicoechea, Applications of electrochemical data analysis by multivariate curve resolution-alternating least squares, Trends Anal. Chem. 88C (2017) 134–166.
[22] G. Mohammadi, K. Rashidi, M. Mahmoudi, H.C. Goicoechea, A.R. Jalalvand, Exploiting second-order advantage from mathematically modeled voltammetric data for simultaneous determination of multiple antiparkinson agents in the presence of uncalibrated interference, J. Taiwan Inst. Chem. Eng. 88 (2018) 49–61.
[23] H. Gampp, M. Maeder, C.J. Meyer, A.D. Zuberbühler, Calculation of equilibrium constants from multiwavelength spectroscopic data—III: Model-free analysis of spectrophotometric and ESR titrations, Talanta 32 (1985) 1133–1139.
[24] H. Abdollahi, V. Mahdavi, Tautomerization equilibria in aqueous micellar solutions: a spectrophotometric and factor-analytical study, Langmuir 23 (2007) 2362–2368.
[25] S. Perez, M.J. Culzoni, G.G. Siano, M.D. Gil Garcia, H.C. Goicoechea, M.M. Galera, Detection of unintended stress effects based on a metabonomic study in tomato fruits after treatment with carbofuran pesticide. Capabilities of MCR-ALS applied to LC-MS three-way data arrays, Anal. Chem. 81 (2009) 8335–8346.
[26] M. Vives, R. Gargallo, R. Tauler, Study of the intercalation equilibrium between the polynucleotide poly(adenylic)-poly(uridylic) acid and the ethidium bromide dye by means of multivariate curve resolution and the multivariate extension of the continuous variation and mole ratio methods, Anal. Chem. 71 (1999) 4328–4337.
[27] C.B. Zachariassen, J. Larsen, F. Van den Berg, R. Bro, A. De Juan, R. Tauler, Comparison of PARAFAC2 and MCR-ALS for resolution of an analytical liquid dilution system, Chemom. Intell. Lab. Syst. 83 (2006) 13–25.
[28] R. Tauler, A. Izquierdo-Ridorsa, E. Casassas, Simultaneous analysis of several spectroscopic titrations with self-modelling curve resolution, Chemom. Intell. Lab. Syst. 18 (1993) 293–300.
[29] R. Tauler, A.K. Smilde, B.R. Kowalski, Selectivity, local rank, three-way data analysis and ambiguity in multivariate curve resolution, J. Chemom. 9 (1995) 31–58.
[30] M. Esteban, C. Arino, J.M. Dıaz-Cruz, M.S. Diaz-Cruz, R. Tauler, Multivariate curve resolution with alternating least squares optimisation: a soft-modelling approach to metal complexation studies by voltammetric techniques, Trends Anal. Chem. 19 (2000) 49–61.
[31] M. Esteban, C. Arino, J.M. Dıaz-Cruz, Chemometrics for the analysis of voltammetric data, Trends Anal. Chem. 25 (2006) 86–92.
[32] R.N. Goyal, A.B. Toth, G. Dryhurst, N.T. Nguyen, A comparison of the peroxidase-catalyzed and electrochemical oxidation of uric acid, Bioelectrochem. Bioenerg. 9 (1982) 39–60.
[33] Y.N. Ni, X. Zhang, S. Kokot, Spectrometric and voltammetric studies of the interaction between quercetin and bovine serum albumin using warfarin as site marker with the aid of chemometrics, Spectrochim. Acta A 71 (2009) 1865–1872.
[34] A.J. Bard, L.R. Faulkner, Electrochemical Methods: Fundamentals and Applications, Second ed., Wiley, New York, 2001.
[35] E. Laviron, Adsorption, autoinhibition and autocatalysis in polarography and in linear potential sweep voltammetry, J. Electroanal. Chem. 52 (1974) 355–393.

[36] H. Heli, N. Sattarahmady, A. Jabbari, A.A. Moosavi-Movahedi, G.H. Hakimelahi, F.Y. Tsai, Adsorption of human serum albumin onto glassy carbon surface-applied to albumin-modified electrode: mode of protein-ligand interactions, J. Electroanal. Chem. 610 (2007) 67–74.
[37] V. Brabec, DNA sensor for the determination of antitumor platinum compounds, Electrochim. Acta 45 (2000) 2929–2932.
[38] X. Ju, Y.K. Ye, Y.L. Zhu, Interaction between nile blue and immobilized single- or double-stranded DNA and its application in electrochemical recognition, Electrochim. Acta 50 (2005) 1361–1367.
[39] S.S. Kalanur, U. Katrahalli, J. Seetharamappa, Electrochemical studies and spectroscopic investigations on the interaction of an anticancer drug with DNA and their analytical applications, J. Electroanal. Chem. 636 (2009) 93–100.
[40] B. Ojiha, G. Das, The interaction of 5-(Alkoxy)naphthalen-1-amine with bovine serum albumin and its effect on the conformation of protein, J. Phys. Chem. B 114 (2010) 3979–3986.
[41] D.M. Charbonneau, H.A. Tajmir-RIAHI, Study on the interaction of cationic lipids with bovine serum albumin, J. Phys. Chem. B 114 (2010) 1148–1155.
[42] J.R. Lakowicz, Principles of Fluorescence Spectroscopy, Second ed., Plenum Press, New York, 1999.
[43] M.A. Khan, S. Muzammil, J. Musarrat, Interaction of genome-linked protein (VPg) of turnip mosaic virus with wheat germ translation initiation factors eIFiso4E and eIFiso4F, Int. J. Biol. Macramol. 30 (2002) 243–249.
[44] G. Sudlow, D.J. Birkett, D.N. Wade, Further characterization of specific drug binding sites on human serum albumin, Mol. Pharmacol. 12 (1976) 1052–1061.
[45] L. Stryer, R.P. Haugland, Energy transfer: a spectroscopic ruler, Proc. Natl. Acad. Sci. U. S. A. 58 (1967) 719–726.
[46] B. Valeur, J.C. Brochon, New Trends in Fluorescence Spectroscopy, Third ed., Springer, Berlin, 2001.
[47] F.L. Cui, J. Fan, J.P. Li, Z.D. Hu, Interactions between 1-benzoyl-4-p-chlorophenyl thiosemicarbazide and serum albumin: investigation by fluorescence spectroscopy, Bioorg. Med. Chem. 12 (2004) 151–157.
[48] B. Valeur, Molecular Fluorescence: Principles and Applications, Wiley, New York, 2001.
[49] A. de Juan, A. Izquierdo-Ridorsa, R. Tauler, G. Fonrodona, E. Casassas, A soft-modeling approach to interpret thermodynamic and conformational transitions of polynucleotides, Biophys. J. 73 (1997) 2937–2948.
[50] J. Jaumot, R. Tauler, MCR-BANDS: a user friendly MATLAB program for the evaluation of rotation ambiguities in multivariate curve resolution, Chemom. Intell. Lab. Syst. 103 (2010) 96–107.
[51] H. Abdollahi, R. Tauler, Uniqueness and rotation ambiguities in Multivariate Curve Resolution methods, Chemom. Intell. Lab. Syst. 108 (2011) 100–111.
[52] R. Tauler, Calculation of maximum and minimum band boundaries of feasible solutions for species profiles obtained by multivariate curve resolution, J. Chemom. 15 (2001) 627–646.
[53] H. Parastar, M. Jalali-Heravi, R. Tauler, Is independent component analysis appropriate for multivariate resolution in analytical chemistry? Trends Anal. Chem. 31 (2012) 134–143.
[54] R.M. Dyson, S. Kaderli, G.A. Lawrance, M. Maeder, A.D. Zuberbühler, Second order global analysis: the evaluation of series of spectrophotometric titrations for improved determination of equilibrium constants, Anal. Chim. Acta 353 (1997) 381–393.
[55] A.R. Jalalvand, Fabrication of a novel and ultrasensitive label-free electrochemical aptasensor for detection of biomarker prostate specific antigen, Int. J. Biol. Macromol. 126 (2019) 1065–1073.
[56] R. Khodarahmi, S. Khateri, H. Adibi, V. Nasirian, M. Hedayati, E. Faramarzi, S. Soleimani, H.C. Goicoechea, A.R. Jalalvand, Chemometrical-electrochemical investigation for comparing inhibitory effects of quercetin and its sulfonamide derivative on human carbonic anhydrase II: theoretical and experimental evidence, Int. J. Biol. Macromol. 136 (2019) 377–385.
[57] A.R. Jalalvand, M.B. Gholivand, H.C. Goicoechea, T. Skov, K. Mansouri, Mimicking enzymatic effects of cytochrome P450 by an efficient biosensor for in vitro detection of DNA damage, Int. J. Biol. Macromol. 79 (2015) 1004–1010.
[58] M.B. Gholivand, A.R. Jalalvand, H.C. Goicoechea, G. Paimard, T. Skov, Surface exploration of a room-temperature ionic liquid-chitin composite film decorated with electrochemically deposited PdFeNi trimetallic alloy nanoparticles by pattern recognition: an elegant approach to developing a novel biotin biosensor, Talanta 131 (2015) 249–258.
[59] M.B. Gholivand, A.R. Jalalvand, H.C. Goicoechea, Computer-assisted electrochemical fabrication of a highly selective and sensitive amperometric nitrite sensor based on surface decoration of electrochemically reduced graphene oxide nanosheets with CoNi bimetallic alloy nanoparticles, Mater. Sci. Eng., C 40 (2014) 109–120.